Journal of
Materials Chemistry A

Accepted Manuscript

This article can be cited before page numbers have been issued, to do this please use: T. Zhou, T. Cheng, S. V. Zybin, W. A. Goddard and F. Huang, *J. Mater. Chem. A*, 2018, DOI: 10.1039/C7TA10998A.

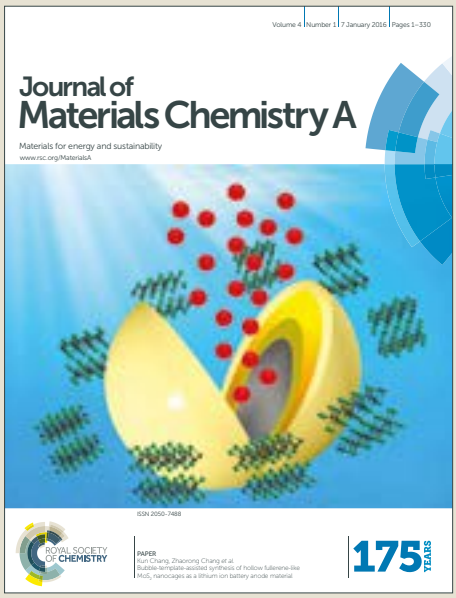

This is an Accepted Manuscript, which has been through the Royal Society of Chemistry peer review process and has been accepted for publication.

Accepted Manuscripts are published online shortly after acceptance, before technical editing, formatting and proof reading. Using this free service, authors can make their results available to the community, in citable form, before we publish the edited article. We will replace this Accepted Manuscript with the edited and formatted Advance Article as soon as it is available.

You can find more information about Accepted Manuscripts in the author guidelines.

Please note that technical editing may introduce minor changes to the text and/or graphics, which may alter content. The journal's standard Terms & Conditions and the ethical guidelines, outlined in our author and reviewer resource centre, still apply. In no event shall the Royal Society of Chemistry be held responsible for any errors or omissions in this Accepted Manuscript or any consequences arising from the use of any information it contains.

ROYAL SOCIETY OF CHEMISTRY

rsc.li/materials-a

View Article Online
DOI: 10.1039/C7TA10998A

Reaction Mechanisms and Sensitivity for Silicon Nitrocarbamate and Related Systems from Quantum Mechanics Reaction Dynamics

Tingting Zhou[a,b] *Tao Cheng,*[b] *Sergey V. Zybin,*[b] *William A. Goddard III,*[b*] *and Fenglei Huang*[c]

[a] *Institute of Applied Physics and Computational Mathematics, Beijing, 100094, P. R. CHINA.*

[b] *Materials and Process Simulation Center, 139-74, California Institute of Technology, Pasadena, California, 91125, USA. E-mail: wag@wag.caltech.edu.*

[c] *State Key Laboratory of Explosion Science and Technology, Beijing Institute of Technology, Beijing, 100081, P. R. CHINA.*

**Email - wag@wag.caltech.edu, wagoddard3@gmail.com*

Abstract: Temperature induced instability is an important issue in developing new molecules and materials, but there is no clear understanding about how molecular structure and crystal packing control sensitivity. This is particularly the case for energetic materials (EM) important in propulsion and detonation. We propose here using the quantum mechanics molecular dynamics (QM-MD) based tempereature programmed reaction dynamics for predicting the relative sensitivity of various materials while simultaneously obtaining the reaction mechanisms underlying to provide guidance in improving materials. We illustrate this for four closely related molecules, pentaerythritol tetranitrate, pentaerythritol tetranitrocarbamate, and their silicon analogs, that have minor intramolecular differences but exhibit different sensitivities experimentally. Our study finds dramatic differences in reaction mechanisms and energy variation under heating that suggest explanations for the different sensitivities. Important here are both the initial decomposition and the secondary reactions between products. The higher sensitivity of the Si analogs originates from the highly exothermic Si–O bond formation as a paramount initial reaction that promotes other reactions, leading to the generations of various intermediates and final products, thus accelerating the decomposition process and energy release. The nitrocarbamates have low sensitivity because their large complex branching impedes the exothermic Si/C–O bond formation and triggers multiple initial endothermic reaction pathways with higher reaction barrier, delaying secondary exothermic reactions and energy release. We find two computational measures that correlate well with sensitivity: the temperatures at which the energy changes from endothermic to exothermic and the total absorbed energy. This study provides mechanistic insight on the molecular and structural determinants controlling the sensitivity of EMs and provides a practical way to predict the relative sensitivity in advance of experimental synthesis and characterization, benefiting the design of novel EMs.

View Article Online
DOI: 10.1039/C7TA10998A

Keywords: reaction mechanism; thermal sensitivity; energetic material; density functional theory; molecular dynamics

1. Introduction

Energetic materials (EMs), including propellants, explosives, and pyrotechnics, are used extensively for a variety of civilian and military applications. Current researches to improve EMs focus on designing and synthesizing novel compounds with high detonation performance (comparable to the benchmark EMs such as cyclotetramethylene-tetranitramine (HMX) and cyclotrimethylene-trinitramine (RDX)) while simultaneously reducing sensitivity for safety considerations.[1-11] However, high energy and low sensitivity requirements are often contradictory, making the development of new EMs difficult and challenging.[1-11] We aim here to provide the synthetic chemists a simple tool for predicting the sensitivity prior to the often complex and time consuming process of synthesizing new generations of EMs.

Sensitivity involves how quickly external stimuli (thermal, impact, friction, electrostatic discharge, or shock) can initiate chemical reactions that lead to decomposition and energy release. This is a crucial factor that determines the safety and affects the manufacture, transportation, application and storage of these materials.[1-4,12] A high priority in designing and evaluating proposed new energetic compounds is to minimizing sensitivity. Therefore, it is very useful to find a way to predict the factors affecting sensitivity in order to quickly explore new generations of EMs.

It is widely accepted that sensitivity depends upon a complex interplay of such factors as molecular structure, crystal packing, packing of grains into the test materials, and the nature of the stimulus.[12-15] Reproducibility of the measured values is notoriously difficult, leading often to contradictory results. At crystal scale, sensitivity is related to molecular packing mode, anisotropy, and crystal quality such as defect, shape, and size.[16-22] At molecular scale, sensitivity is strongly dependent on molecular composition and geometry configuration.[1,23-28] For example, sila-pentaerythritol tetranitrate (Si-PETN) shows a dramatically increased sensitivity compared to its carbon analog pentaerythritol tetranitrate (PETN), although the two molecular structures are nearly identical to each other besides the central atom (silicon vs. carbon).[23-25] δ- and β-HMX have the same molecular composition but different geometry configurations, and the former is more sensitive than the latter.[26] Thus even for single crystals the relation between sensitivity and material characteristics is complex and not understood. This

View Article Online
DOI: 10.1039/C7TA10998A

becomes even more complex at the mesoscale, where microstructure including grain boundary, interface, surface, and voids lead to additional influence on the sensitivity of polycrystalline EMs.[12,29,30,31-33]

Recently, the Klapötke group synthesized several nitrocarbamate compounds as potential EMs including the neo-pentane derivative pentaerythritol tetranitrocarbamate (PETNC) and its silicon analog Si-PETNC.[27,28] In comparison with the well-known and widely used explosive PETN, PETNC shows an increased thermal stability as well as lower sensitivities against friction and impact.[27] Si-PETNC also exhibits higher thermal stability and is much less sensitive to impact as well as friction compared to Si-PETN.[28] Si-PETNC is more sensitive than its carbon analog PETNC and matches roughly with the nitrate ester PETN.[28]

Due to the complexity of factors that might affect sensitivity, previous theoretical studies on predicting sensitivity have generally tried to correlate with a single molecular or crystal property of EMs, such as oxygen balance, molecular electronegativity, partial atomic charge, electrostatic potentials, weakest bond dissociation energy, band gap, free space per molecule, crystal packing mode, etc.[34-45] Despite significant efforts and many suggested empirical correlations, no clear understanding has been achieved of the relationships between sensitivity of materials, their molecular and crystalline structures, and chemical properties.[36,46]

We consider that the four compounds, Si-PETN, PETN, Si-PETNC, and PETNC, provide a good challenge to develop an understanding of the molecular and structural determinants controlling their sensitivity to external stimuli. This is because PETN, PETNC, and Si-PETNC have exactly the identical space group $P\bar{4}21c$ with minor differences in molecular structure.[27,28,47] Although the experimental crystal structure for Si-PETN is unavailable, we assume that it is also the case since the molecular structures for Si-PETN and PETN are nearly the same besides the central atom.[23] The molecular and crystal structures for the four EMs are shown in Fig. 1. Our previous theoretical studies[24,25] on the decomposition mechanisms of PETN and Si-PETN elucidated how the replacement of central C by Si dramatically increases the sensitivity of Si-PETN. In the current work, we use quantum mechanics molecular dynamics (QM-MD) to predict the thermal decomposition mechanisms and sensitivity of condensed phase Si-PETN, PETN, Si-PETNC, and PETNC.

View Article Online
DOI: 10.1039/C7TA10998A

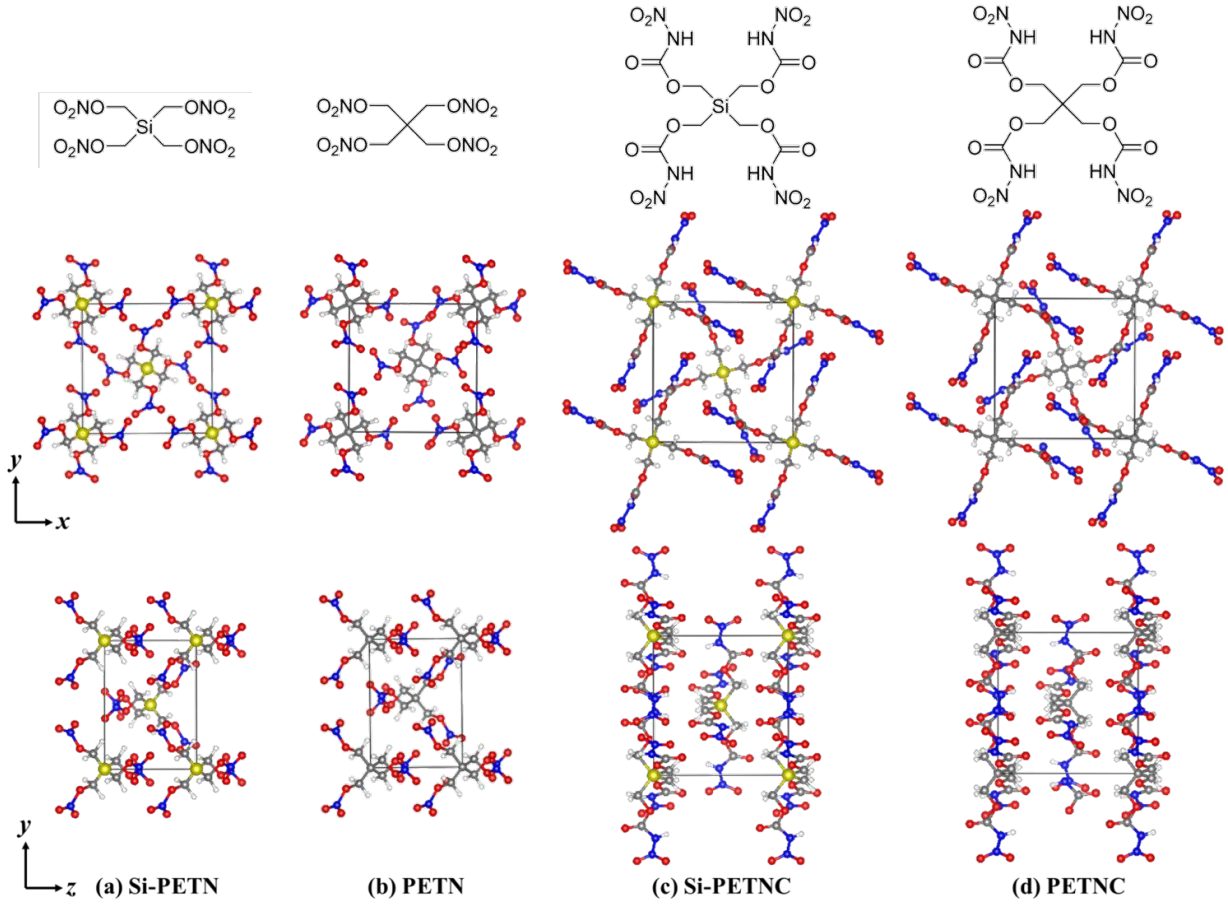

Fig. 1 The molecular and crystal structures for PETN, Si-PETN, PETNC, and Si-PETNC. The crystal structures shown on the top are viewed along *c* axis, and the ones on the bottom are along *a* axis. The C, H, N, O, and Si atoms are represented by gray, white, blue, red, and yellow balls, respectively.

We here aim to uncover the complex chemical processes underlying thermal initiation and the reasons for the lower sensitivity of nitrocarbamate compounds and for the higher sensitivity of silicon analogs. Then we want to find a simple method to predict the relative sensitivity of EMs. The problems associated with characterizing and measuring sensitivity suggest that seeking precise structure/activity correlations is unrealistic except on a very limited scale.[37] Accordingly, our goal is to try to understand the molecular determinants that influence sensitivity, and then to make meaningful predictions of relative sensitivities. This should help provide clues useful for understanding sensitivity of other systems to aid molecular design of novel EMs with tailored properties. Moreover, the chemical reaction mechanism and kinetics including the energy release are essential to developing thermochemical models useful in hydrodynamic simulations of these materials.

View Article Online
DOI: 10.1039/C7TA10998A

This is the first report of QM-MD studies of the reaction mechanisms and thermal sensitivity of solid Si-PETN, PETN, Si-PETNC, and PETNC. We used the PBE-D3 flavor of the generalized gradient approximation to density functional theory (DFT) with periodic boundary conditions. The details of computational methods are given in section 2. The simulated results are presented and discussed in section 3. Conclusions are drawn in section 4.

2. Methodology

The QM calculations use the interatomic forces calculated in the framework of density functional theory (DFT),[48] where exchange and correlation are treated with the generalized gradient approximation (GGA) using the Perdew–Burke–Ernzerhof (PBE) functional form.[49] The London dispersion was corrected using the D3 method with Becke-Jonson damping.[50] The Vienna Ab-initio Simulation Package (VASP)[51] ported to GPU was employed to perform these periodic QM simulations.

Since there is no experimental crystal structure for Si-PETN and the difference between Si-PETN and PETN molecule is the central atom type, we first replaced the center C in PETN with Si and optimized the molecular and crystal structure using conjugate gradients methodology to obtain the Si-PETN crystal. The energy cutoff for the plane wave expansion was set to 600 eV. Convergence is reached if the energy and force differences are within 1×10^{-6} eV for electronic iterations and 1×10^{-4} eV/Å for ionic relaxations, respectively. Reciprocal space was sampled with the Γ-centered Monkhorst-Pack scheme using $3 \times 3 \times 5$ gamma points. For consistency, the other three experimental crystal structures were also relaxed at the same computational level. The cell parameters of the optimized crystal structures are summarized in Table S1 of the Electronic Supplementary Information (ESI), showing excellent agreement with available experimental and theoretical results.[33,34,47,53] These optimized unit cells were then replicated by twice so that each has four molecules per periodic cell for the MD simulations.

The DFT-MD simulations were then performed to investigate the reaction mechanisms of thermal decomposition under heating. The systems were first heated from 20 K to 300 K within 2 ps, followed by equilibration at 300 K for 2 ps. They were finally heated continuously from 300 K to 3000 K over 20 ps (at a heating rate of 135 K/ps). NVT ensemble (constant temperature, constant volume, and constant number of atoms) was used, and the temperature was controlled using the Nose-Hoover thermostat with a time constant of 50 fs. A time step of 1 fs for integrating the equations of motion was applied. The MD trajectories were saved every 10 fs and used to analyze reaction mechanisms. The high

View Article Online
DOI: 10.1039/C7TA10998A

temperatures used in these MD simulations allow many reactions to be observed within the practical time scale of DFT-MD of 20 ps. For these supercell DFT-MD simulations, the energy cutoff for the plane wave expansion was reduced to 500 eV. The convergence criteria were 1×10^{-5} eV for energy difference and 1×10^{-3} eV/Å for force difference. Only the gamma point of reciprocal space was sampled.

To identify reaction products formed during thermal decomposition, we determined the atom connectivity using bond order cutoffs. The algorithm is the same as that used in previous studies of reactive molecular dynamics simulations.[52] Any two fragments are considered as separate molecules if all bonds between them have bond orders smaller than the cutoff values. After determining the molecular fragments, the molecular recognition algorithm assigns a unique identification number to each fragment to trace the reaction pathways. The cutoffs for various atom pairs (tabulated in Table S2-S5 of the ESI) are confirmed by comparing the analyzed products with the molecular structures in the decomposed crystals from the MD trajectories. We used a time window of 0.2 ps to avoid confusion due to short-term fluctuations in the bonds above and below the cutoff. That is the bond must be maintained for at least 0.2 ps to be considered as a bond.

3. Results and discussion

3.1 Reaction Mechanisms for the Nitro Esters Si-PETN and PETN

3.1a Si-PETN

The initiation of thermal decomposition of Si-PETN occurs through O–NO_2 bond cleavage when temperature increases to 1543 K (t = 9.21 ps), leading to the formation of NO_2. Then the Si–CH_2O bond breaks immediately after NO_2 dissociation, generating CH_2O at 1549 K (t = 9.25 ps). Next we find the formation of Si–O bond as the temperature reaches 1562 K (t = 9.35 ps). The mechanisms of these first three initial reactions are illustrated in Fig. 2, showing that for all the four intact Si-PETN molecules, the first reaction step is always O–NO_2 bond rupture followed by Si–CH_2O bond breakage in the same branch. Previous static QM calculations on single Si-PETN molecule[24] suggested that the barrier for CH_2O dissociation is 48.2 kcal/mol, which is 12.6 kcal/mol higher than that for NO_2 release, explaining why CH_2O always forms after NO_2.

View Article Online
DOI: 10.1039/C7TA10998A

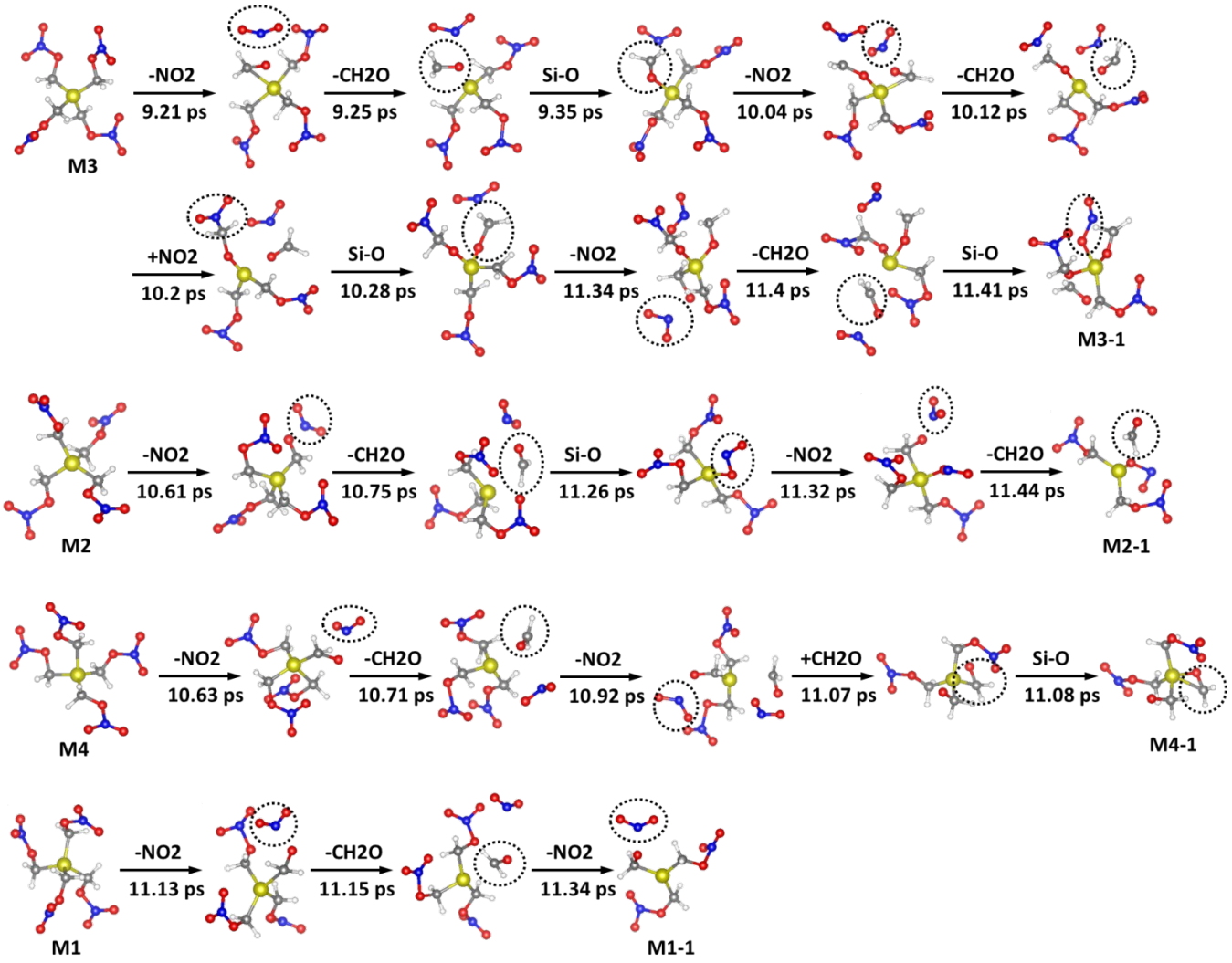

Fig. 2 Reaction process of initial reactions during the thermal decomposition of Si-PETN. The C, H, N, O, and Si atoms are represented by gray, white, blue, red, and yellow balls, respectively. The four intact Si-PETN molecules are represented by M1, M2, M3, and M4. The partially decomposed Si-PETN molecules after these reactions are represented by M1-1, M2-1, M3-1, and M4-1.

The Si–O bond formation is paramount in the initial reactions since it leads to massive energy release (-44.5 kcal/mol),[24] which can promote other reactions to accelerate the decomposition process. The first two Si–O bonds (t = 9.35, 10.28 ps) are formed due to the attraction between the central Si and the O in the dissociated CH_2O. We observe the bending of Si–CH_2–O after NO_2 dissociation and before CH_2O elimination, resulting in the extension of the Si–C bond while decreasing the distance of the O from the central Si. The subsequent CH_2O dissociation is similar to the transition state of the rearrangement of Si–CH_2–O predicted from QM calculations.[24] The Si–O bond formed at 11.08 ps involves the

View Article Online
DOI: 10.1039/C7TA10998A

rearrangement of Si–CH_2–O in the branch after losing NO_2. The attraction between the central Si and one O in the dissociated NO_2 leads to formation of Si–O bonds at 11.26 and 11.41 ps.

The number of Si–O bonds increases continuously as temperature increases and a rapid increment begins after the temperature approaches 1796 K (t = 11.08 ps), as shown in Fig. S1 (a). The reaction pathways leading to the formation of Si–O bonds are collected in Table 1 and the molecular structures before and after Si–O bond formations are illustrated in Fig. S2 of the ESI, from which detailed information about the reaction mechanisms can be derived. Mechanism one is the attraction between the central Si and the O in dissociation fragments such as CH_2O, NO_2, NO_3, CNO_3, and CHO_2. The Si–O bonds formed at 9.35, 10.28, 12.59 ps arise from the attraction between Si and O in the dissociated CH_2O. The attraction between Si and one O in the split NO_2 leads to formation of Si–O bonds at 11.26, 11.41, 12.07, 12.29, and 13.22 ps. The Si–O bonds formed at 13, 13.49, and 14.27 ps arise from the attraction between Si and O in the dissociated NO_3, CNO_3, and CHO_2, respectively. Mechanism two involves the rearrangement of Si–CH_2–O in the branches after losing NO_2, forming the Si–O bonds at 11.08 and 11.76 ps. Mechanism three is the attraction between Si and one O in –NO_2. The Si–O bond formed at 11.39 ps is due to intermolecular attraction and the ones at 12.13 and 12.3 ps are due to intramolecular attraction. In the fragment with two Si, the O in the Si–O bond formed at 12.3 ps also bonds to the other Si at t = 12.48 ps. The attraction between the central Si and the O in dissociation fragments plays the dominant role in the formation of Si–O bond. After losing one branch (NO_2 and CH_2O) in the Si-PETN molecule, the central Si atom connecting with three atoms becomes more active than the original state with four atoms. And the cleavage of the branch leaves more free space and exposes the central Si to other fragments, making it easier to attract the O in dissociated products and form Si–O bond.

Table 1 Reaction pathways and the corresponding time and temperature leading to Si–O bond formation in Si-PETN crystal during heating process

products	reaction pathways	t (ps)	T (K)
Si–O bond	CH_2O (7) + $C_3H_6N_3O_9Si$ (8) → $C_4H_8N_3O_{10}Si$ (9)	9.35	1562
	$C_3H_6N_3O_9Si$ (13) + CH_2O (12) → $C_4H_8N_3O_{10}Si$ (15)	10.28	1688
	$C_4H_8N_2O_8Si$ (26) → $C_4H_8N_2O_8Si$ (27)	11.08	1796
	$C_3H_6N_3O_9Si$ (23) + NO_2 (16) → $C_3H_6N_4O_{11}Si$ (34)	11.26	1820
	$C_3H_6N_2O_7Si$ (39) + $C_3H_6N_2O_7Si$ (29) → $C_6H_{12}N_4O_{14}Si_2$ (41)	11.39	1838
	$C_3H_6N_2O_7Si$ (43) + NO_2 (10) → $C_3H_6N_3O_9Si$ (44)	11.41	1840
	$C_6H_{12}N_2O_{11}Si_2$ (72) → $C_6H_{12}N_2O_{11}Si_2$ (77)	11.76	1888
	$C_6H_{11}N_2O_{11}Si_2$ (83) + NO_2 (35) → $C_6H_{11}N_3O_{13}Si_2$ (90)	12.07	1929

View Article Online
DOI: 10.1039/C7TA10998A

$C_2H_4NO_5Si$ (95) → $C_2H_4NO_5Si$ (97)	12.13	1938
$C_5H_9NO_{10}Si_2$ (105) + NO_2 (18) → $C_5H_9N_2O_{12}Si_2$ (111)	12.29	1959
$C_5H_9N_2O_{12}Si_2$ (111) → $C_5H_9NO_9Si_2$ (112) + NO_3 (113)	12.30	1961
$C_4H_{10}NO_8Si_2$ (120) → $C_3H_8NO_7Si_2$ (122) + CH_2O (121)	12.48	1985
CH_2O (32) + $C_2H_2O_3Si$ (79) → $C_3H_4O_4Si$ (123)	12.59	2000
$C_3H_8NO_7Si_2$ (122) + NO_3 (113) → $C_3H_8N_2O_{10}Si_2$ (131)	13.00	2055
CH_2O_3Si (142) + NO_2 (38) → CH_2NO_5Si (149)	13.22	2085
CH_2NO_5Si (149) + CNO_3 (158) → $C_2H_2N_2O_8Si$ (160)	13.49	2121
$C_2H_6NO_5Si$ (210) + CHO_2 (172) → $C_3H_7NO_7Si$ (211)	14.27	2226

The numbers in parentheses are the identifications (ID) of fragments.

Static QM calculations[24] suggested that the Si–O bond formation via carbon-silyl nitro-ester rearrangement (R3Si–CH_2–O–R2 → R3Si–O–CH_2–R2) should be the first reaction step due to its lower barrier than O–NO_2 bond cleavage (reaction enthalpy: 32.0 vs. 35.6 kcal/mol). However, our QM dynamical simulation under constant heating rate shows that Si–CH_2–O rearrangement occurs after O–NO_2 bond breaking. This is because the rearrangement has a very tight transition state (very low entropy) which is disfavored at higher temperature. Experiments exposing the crystal to a high-energy laser, high-energy fracture, or high pressure found that Si–C/C–C and C–O bonds the first to break, which was interpreted to suggest that O–NO_2 bond is relatively strong than these other bonds.[54-56] In contrast, we find that slower thermal decomposition leads to O–NO_2 bond rupture as the initial step, which was also observed for low-energy fracture or low energy laser at ambient pressures.[55,57]

As temperature increases above 1850 K, we observe the formation of NO, H, and HONO. The NO_2 attracted by the central Si atom breaks one O–N bond, leading to the elimination of NO at an early stage. The NO formed at a later time is due to the further decompositions of other products (e.g., HONO, N_2O_3, the fragment with two Si formed by the combination of two partially decomposed Si-PETN molecules). H atoms are mainly dissociated from the partially decomposed Si-PETN and from the decompositions of other products (e.g., HONO, HNO). The secondary reaction between dissociated NO_2 and H contributes greatly to the formation of HONO, which is also split from the fragment with two Si and from the partially decomposed Si-PETN. Although QM calculations of the adiabatic energy surfaces suggested that HONO might be an initial reaction, because the reaction barrier is only 3.8 kcal/mol higher than that for NO_2 dissociation,[24] our MD simulations indicate that HONO does not eliminate directly from the original Si-PETN molecule, and it forms much later and at a higher temperature than NO_2, CH_2O, and Si–O bond formations.

The onsets of various secondary exothermic reactions between decomposition products lead later to the formation of many intermediate products (such as HO, CH_2O_2, HNO, CHO_2, CNO, and CHNO) and

View Article Online
DOI: 10.1039/C7TA10998A

final products (such as CO, H_2O, N_2O, and CO_2). These exothermic reactions are critical since they contribute to the energy release that accelerates the decomposition process. The observed rate increase as the decomposition continues have showed that reactions between decomposition products accelerates decomposition with possible autocatalytic effects.[58-60] The time evolutions of major reaction products formed during the thermal decomposition of Si-PETN are presented in Fig. S1 of the ESI.

3.1b PETN

In the heating induced decomposition of PETN, the first reaction step is also O–NO_2 bond fission when temperature approaches 2078 K (t = 13.17 ps), which is ~540 K higher (~4 ps later) than that for Si-PETN, indicating that PETN is much more stable. The next reactions are the eliminations of HONO and H at the same time (T = 2087 K, t = 13.24 ps), immediately after the dissociation of NO_2. Very quickly in another 0.14 ps (T = 2097 K, t = 13.31 ps), we find that C–CH_2O bond breaks leading to the formation of CH_2O. The reaction processes regarding to the four initial reaction products are illustrated in Fig. 3, showing that the initiation of thermal decomposition is always through O–NO_2 bond cleavage for all the four intact PETN molecules. The subsequent reaction between dissociated NO_2 and the H in partially decomposed PETN or dissociated H leads to the formation of HONO. Both H and CH_2O are eliminated from the branch after losing NO_2. Static QM calculations on a single PETN molecule[24] found that the barrier for HONO elimination is essentially the same as for O–NO_2 bond cleavage (39.2 vs. 39.0 kcal/mol). However, our dynamical simulation under heating shows that HONO is always formed after NO_2 and is not dissociated directly from the intact PETN molecule. The barrier for CH_2O dissociation is about 10 kcal/mol higher (49.1 kcal/mol),[24] which is consistent with the delayed occurrence compared to the formation of NO_2 and HONO.

View Article Online
DOI: 10.1039/C7TA10998A

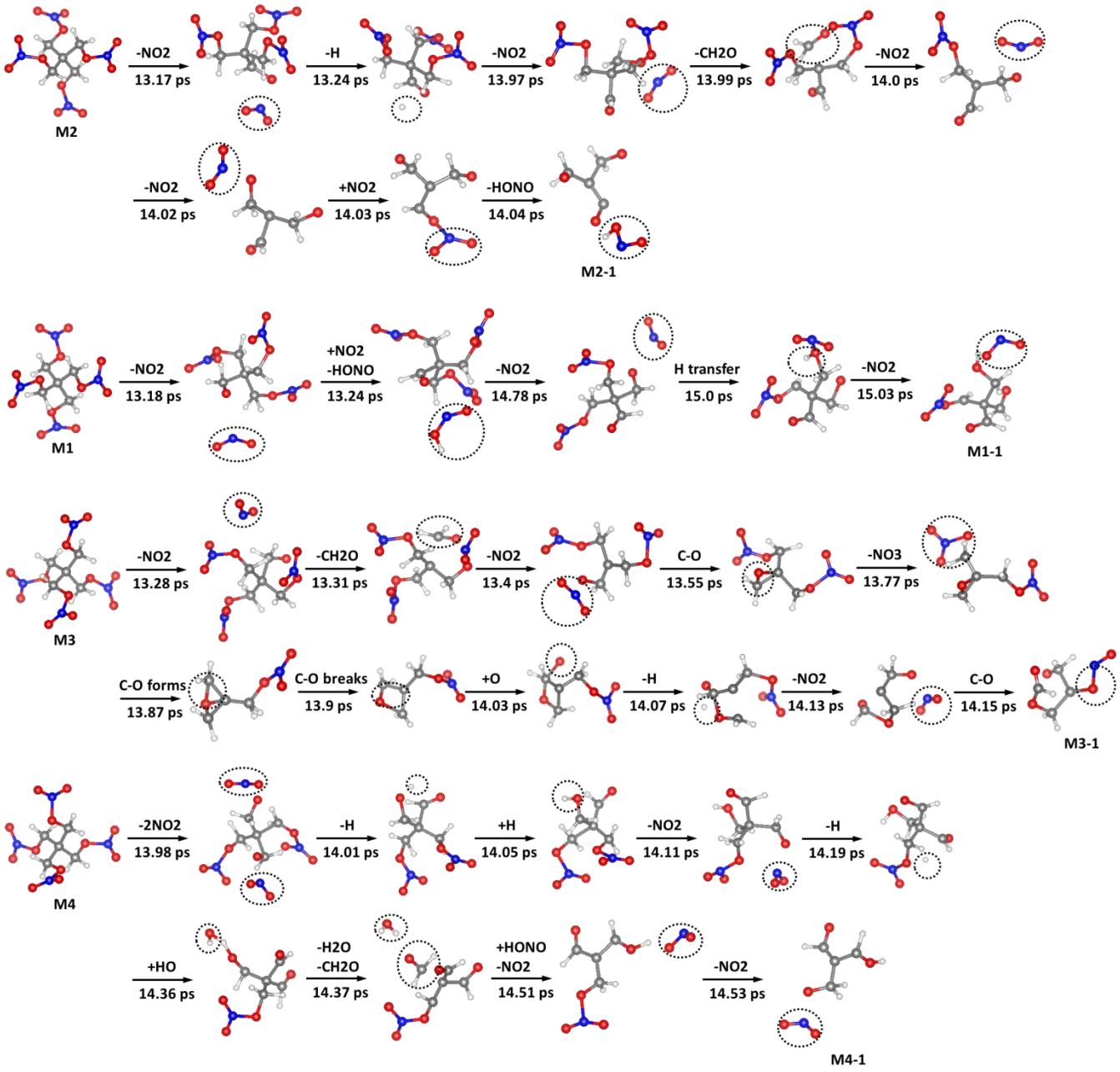

Fig. 3 Reaction process of initial reactions during the thermal decomposition of PETN. The C, H, N, and O atoms are represented by gray, white, blue, and red balls, respectively. The four intact PETN molecules are represented by M1, M2, M3, and M4. The partially decomposed PETN after these reactions are represented by M1-1, M2-1, M3-1, and M4-1.

The rearrangement of C–CH_2–O (R3C–CH_2–O–R2 → R3C–O–CH_2–R2) leading to the formation of C–O bond was suggested to be impossible due to the extremely high barrier (80.1 kcal/mol).[24] Indeed, we only observe one similar rearrangement at 2129 K (t = 13.55 ps) in the branch after losing NO_2 in the partially decomposed PETN (molecular ID: M3), as illustrated in Fig. 3. The central C atom

View Article Online
DOI: 10.1039/C7TA10998A

simultaneously bonds to the C and O in the $–CH_2O$, forming four bonds. After 0.32 ps, The C atom belonging to $–CH_2$ in another branch also bonds to the O in $–CH_2O$, leading to the immediate rupture of the C–O bond formed via $C–CH_2–O$ rearrangement. The second C–O bond is formed at 2210 K (t = 14.15 ps) through the attraction between the central C and one O in the dissociated NO_2 in M3. These are the only two C–O bonds formed during the whole decomposition process of PETN. Therefore, C–O bond formation does **not** play an important role in the decomposition of PETN, although this reaction is exothermic (-13.5 kcal/mol[24]). This is the significant difference in the initial reactions between Si-PETN and PETN. For Si-PETN, the formation of many Si–O bonds releases a great deal of energy, dramatically accelerating the decomposition process and dramatically enhancing the sensitivity of Si-PETN.

When temperature increases higher than 2200 K, the formation of NO, HNO, and HO are observed. The further decompositions of PETN moieties and initial products such as HONO and NO_2 generate NO. The secondary reaction between NO and the released H or the H in other products leads to the formation of HNO. HO is mainly generated from the decomposition of HONO. Other intermediate products, including CHO_2, CH_2O_2, and N_2O_2, are formed later due to secondary reactions between products and the further decompositions of other fragments. The thermal decomposition of PETN generates such final products as H_2O, CO_2, CO, N_2O, and N_2. The time evolutions of major reaction products formed during the thermal decomposition of PETN are plotted in Fig. S3 of the ESI.

3.2 Reaction Mechanisms for the Nitrocarbamates Si-PETNC and PETNC

3.2a Si-PETNC

The first reaction step for Si-PETNC is intermolecular hydrogen transfer between two Si-PETNC molecules (M2 and M3), as shown in Fig. 4. The intermolecular H transfer starts as the temperature reaches 1676 K (t = 10.19 ps). The O belonging to –CO in one Si-PETNC attracts the H belonging to –NH in an adjacent Si-PETNC, forming Si-PETNC-H and Si-PETNC+H simultaneously. Then, one O pertaining to $–NO_2$ in Si-PETNC-H attracts the H pertaining to –NH in Si-PETNC+H at 1685 K (t = 10.26 ps), leading to formation of two new Si-PETNC molecules with a modified molecular structure compared to the intact Si-PETNC molecule. After 0.4 ps (t = 10.66 ps, T= 1739 K), the H attracted by $–NO_2$ transfers back to its donor and the H captured by –CO also bonds to its donor, resulting in the formation of a homo-dimer. This dimer disappears immediately due to the bond breaking of N–H (t = 10.67 ps, T = 1740 K), forming again Si-PETNC-H and Si-PETNC+H. After 0.14 ps (t = 10.81 ps, T =

View Article Online
DOI: 10.1039/C7TA10998A

1759 K), the H pertaining to –NH in another branch of Si-PETNC-H transfers to the O pertaining to –CO in another branch of Si-PETNC+H, leading to the generations of Si-PETNC-2H and Si-PETNC+2H. This H immediately transfers back to its donor and connects with one O in $–NO_2$, forming Si-PETNC-H and Si-PETNC+H for the third time (t = 10.82 ps, T = 1761 K). At t = 11.27 ps (T = 1821 K), the H connected with –CO in Si-PETNC+H also bonds to its donor, forming a hetero-dimer. The O–H bond breaks immediately, resulting in two Si-PETNC molecules (t = 11.28, T = 1823 K). At this point, the intermolecular hydrogen transfer process is completed. In summary, the H transfer is mainly between –NH and –CO or between –NH and $–NO_2$. The final configurations of the two Si-PETNC molecules after intermolecular H transfer are: one Si-PETNC (M3) recovers back to the original configuration and in another Si-PETNC (M2) the H initially connected with –N bonds to one O in $–NO_2$. We did not observe such H transfer for the other two Si-PETNC molecules (M1 and M4).

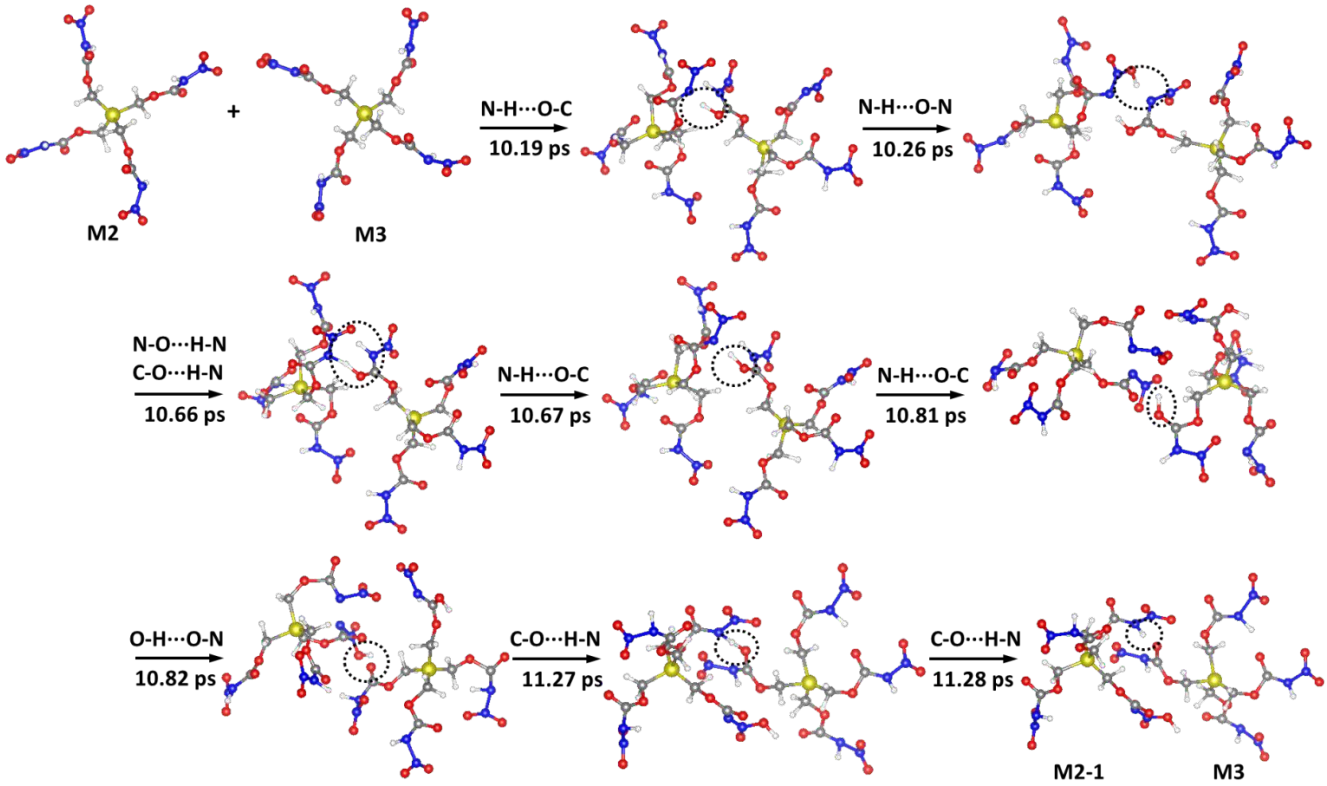

Fig. 4 Reaction process of intermolecular H transfer during the thermal decomposition of Si-PETNC. The C, H, N, O, and Si atoms are represented by gray, white, blue, red, and yellow balls, respectively. The intermolecular hydrogen transfer occurs between two Si-PETNC molecules, M2 and M3. After H transfer, M3 recovers back to the original configuration and M2 converts to M2-1.

View Article Online
DOI: 10.1039/C7TA10998A

As temperature increases above 1966 K (t = 12.34 ps), intramolecular hydrogen transfer between –OH and –CO occurs in the Si-PETNC molecule with the new configuration (M2-1). As shown in Fig. 5, the H bonding to one O in $–NO_2$ also connects with the adjacent O pertaining to –CO in the same branch. Then, the original H–O bond breaks and the H transfers entirely to the O in –CO at 1994 K (t = 12.55 ps). After 2.55 ps (t = 15.1 ps, T = 2339 K), the H transfers back to its donor and this molecular configuration remains until the onset of $N–NO_2$ bond breaking in another branch when temperature reaches 2447 K (t = 15.9 ps). The intramolecular H transfer neither promotes HONO elimination nor HO dissociation.

Although H transfer occurs very early in the decomposition process of Si-PETNC, it does not catalyze other reactions. We did not observe any other reactions during the procedure of intermolecular or intramolecular H transfer and the occurrences of the following decomposition reactions for both the two Si-PETNC molecules are later than the other two Si-PETNC molecules (M1 and M4) without H transfer. As shown in Fig. 5, the decomposition of M1 begins at 12.72 ps and the corresponding temperature is 2017 K, which is ~3 ps earlier and the temperature is ~400 K lower than those for M2 and M3. The decomposition of M4 starts ~0.7 ps earlier and the temperature is ~100 K lower than those for M2 and M3. Therefore, we consider that the back and forth H transfer as initial reaction does **not** accelerate the decomposition of Si-PETNC.

View Article Online
DOI: 10.1039/C7TA10998A

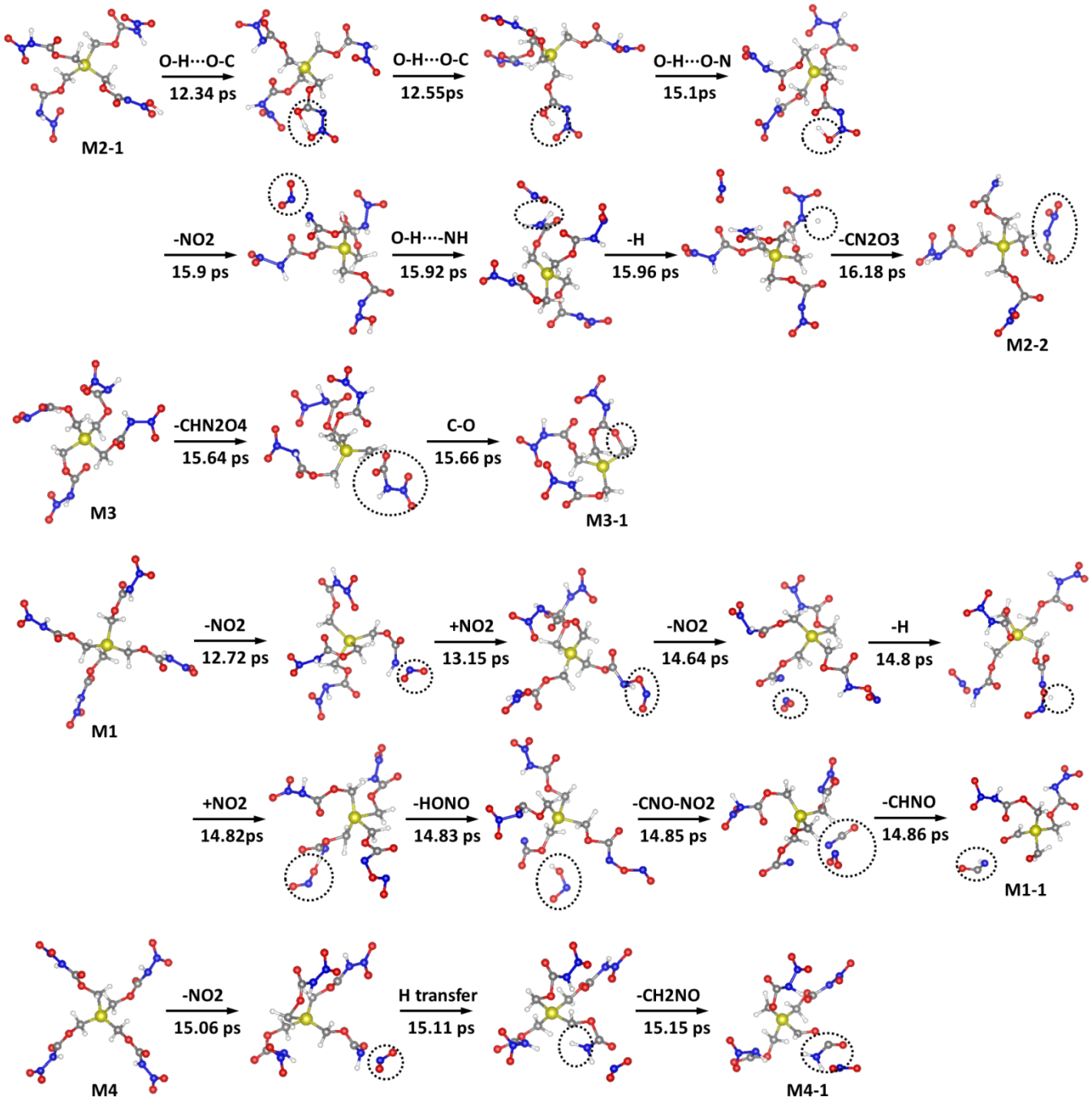

Fig. 5 Reaction process of initial reactions during the thermal decomposition of Si-PETNC. The C, H, N, O, and Si atoms are represented by gray, white, blue, red, and yellow balls, respectively.

The initiation of M3 decomposition occurs via CH_2–O bond rupture dissociating CHN_2O_4, while the decomposition of the other three Si-PETNC molecules begins through N–NO_2 bond cleavage forming NO_2. The first dissociated NO_2 at 12.72 ps is consumed after 0.43 ps due to the bonding between the O and the N in –NH. This branch further dissociates H, NO_2, and CNO during the next 1.7 ps. The second

View Article Online
DOI: 10.1039/C7TA10998A

NO_2 is eliminated from another branch in the same Si-PENC molecule at 14.64 ps (T = 2276 K), which is quickly consumed due to the bonding between the O and the H in –NH, favoring the immediate dissociations of HONO and CHNO from this branch. Therefore, the reactions following N–NO_2 bond cleavage include the dissociations of H, HONO, CNO, and CHNO. These reactions occur sequentially and with very short time intervals, indicating that they are closely correlated with each other. For some reactions, the product of the previous step is the reactant of the next step. The reaction details about these initial products and their evolutions with temperature/time are described in Fig. S4 of the ESI.

As the temperature increases above 2353 K (t = 15.21 ps), we see Si–O bond formation. The exothermicity of this reaction makes it critical in the initial decomposition process. The number of the Si–O bond increases continuously with temperature increase, with a more rapid increment after 2596 K (t = 17.01 ps) as shown in Fig. S4 (a) of the ESI. It reaches the maximum of 13 at 2811 K (t = 18.6 ps) and then decreases to 11 over the next 1.4 ps. The reaction pathways regarding to Si–O bond formation are tabulated in Table 2 and the molecular structures before and after Si–O bond formation are shown in Fig. S5 of the ESI. The mechanisms for Si–O bond formation in Si-PETNC are similar to those in Si-PETN: the rearrangement of Si–CH_2–O in the branch after losing –$CONHNO_2$, the attraction between the central Si and the O in dissociated fragments, and the intermolecular attraction between the Si and the O in –CH_2O. Mechanism one leads to the formation of Si–O bond at 15.21 ps. The Si–O bonds formed at 15.49 and 17.75 ps are due to the Si attracting the O in dissociated HO. The attractions between Si and the O in the dissociated CH_2O lead to formation of Si–O bonds at 16.33 and 17.87 ps. The Si–O bonds formed at 16.48, 16.8, 17.54, 17.61, 17.68, 18.19, and 18.60 ps arise from attractions between Si and one O in CHN_2O_4, $C_3H_4NO_4$, HONO, NO_2, $C_2H_2NO_2$, CH_2O_2, and C_2H_3O, respectively. The Si in the thoroughly decomposed Si-PETNC (M2) attracts the O belonging to –CH_2O in the adjacent Si-PETNC residue (M3), forming a Si–O bond at 17.21 ps. The attraction between the central Si and the O in dissociated products dominates the formation of Si–O bond for Si-PETNC, the same as that for Si-PETN.

Table 2 Reaction pathways and the corresponding time and temperature leading to Si–O bond formation in Si-PETNC crystal during heating process

products	reaction pathways	t (ps)	T (K)
Si–O bond	$C_{13}H_{19}N_9O_{21}Si_2$ (49) → $C_{13}H_{19}N_9O_{21}Si_2$ (51)	15.21	2353
	$C_4H_6N_2O_6Si$ (70) + HO (66) → $C_4H_7N_2O_7Si$ (71)	15.49	2391
	CH_2O (106) + CH_4O_3Si (134) → $C_2H_6O_4Si$ (142)	16.33	2505
	$C_4H_7N_2O_6Si$ (150) + CHN_2O_4 (126) → $C_4H_7N_2O_7Si$ (155) + CHN_2O_3 (158)	16.48	2525

View Article Online
DOI: 10.1039/C7TA10998A

$C_3H_4NO_4$ (191) + $C_3H_4N_2O_3Si$ (177) → C_2HNO_2 (192) + $C_4H_7N_2O_5Si$ (193)	16.80	2568
C_2H_4OSi (222) + $C_5H_8O_4Si$ (231) → $C_7H_{12}O_5Si_2$ (249)	17.21	2623
$C_5H_3N_3O_7Si$ (289) + HONO (181) → $C_5H_4N_4O_9Si$ (291)	17.54	2668
$C_5H_{10}O_2Si_2$ (281) + NO_2 (182) → $C_5H_{10}NO_4Si_2$ (306)	17.61	2677
$C_2H_2NO_2$ (299) + $CHNO_4Si$ (307) → $C_3H_3N_2O_6Si$ (317)	17.68	2687
$C_6H_{11}NO_6Si_2$ (308) + HO (309) → $C_6H_{12}NO_7Si_2$ (323)	17.75	2696
CH_2O (251) + $C_6H_{12}NO_7Si_2$ (323) → $C_7H_{14}NO_8Si_2$ (333)	17.87	2712
$C_7H_{14}N_2O_9Si_2$ (364) + CH_2O_2 (268) + NO_3 (353) → $C_8H_{15}N_2O_{11}Si_2$ (366) + HNO_3 (365)	18.19	2756
$C_5H_8O_9Si_2$ (399) + C_2H_3O (389) → $C_7H_{11}O_{10}Si_2$ (411)	18.60	2811

The numbers in parentheses are the identifications (ID) of the fragments.

For Si-PETNC, the formation of Si–O bond begins later and at a higher temperature than the dissociations of NO_2, H, HONO, CNO, and CHNO. Moreover, all Si–O bonds are formed in the partially decomposed Si-PETNC, most of which are highly decomposed. In comparison with Si-PETN, the Si–O bond formation in Si-PETNC begins at a temperature of ~800 K higher (~5.9 ps later) and the number is less. As shown in Fig. 1, the branch in the original Si-PETNC molecule is much longer than that for Si-PETN, making it more difficult to bend and form a five-coordinate Si as a transition state of Si–CH_2–O rearrangement. This large branch also impedes contacts between the central Si and dissociated fragments, therefore, most of the attractions between the Si and the O in dissociated fragments occur in the highly decomposed Si-PETNC at a later time. Consequently, the roles of Si–O bond formation in initial reactions and in enhancing the sensitivity for Si-PETNC are much less significant than for Si-PETN.

With the continuous increase in temperature, we observe HO, NO, CHN_2O_4, CH_2O, and CH_2O_2. The decomposition of initial product HONO contributes significantly to the formation of HO and NO. HO is also generated from the further decomposition of Si-PETNC moieties and the secondary reactions between other products. NO is also formed due to the decompositions of NO_2, Si-PETNC moieties, and the fragment with two Si. CHN_2O_4 is first dissociated from Si-PETNC (M3) and then from further decomposition of Si-PETNC after losing H, NO_2, and CHNO. We do not consider CHN_2O_4 as a crucial initial product since it forms later than other initial products and the amount is small. CH_2O and CH_2O_2 are formed mainly due to the decompositions of and the secondary reactions between other products. Compared to Si-PETN, CH_2O forms at a much higher temperature and the reaction mechanisms are significantly different for Si-PETNC. The final products formed during the thermal decomposition process of Si-PETNC include H_2O, CO, N_2O, CO_2, and N_2. The time evolutions of major reaction products formed during the thermal decomposition of Si-PETNC are shown in Fig. S4 of the ESI.

View Article Online
DOI: 10.1039/C7TA10998A

3.2b PETNC

The initial reactions during the thermal decomposition of PETNC include the dissociations of $C_2H_3N_2O_4$ and CHN_2O_4, hydrogen transfer, and the formations of H, NO_2, $C_2H_3NO_2$, and CHNO, as shown in Fig. 6. For M1, the first reaction step is the dissociation of $C_2H_3N_2O_4$ due to C–CH_2 bond fission when temperature increases to 2120 K (t = 13.48 ps). $C_2H_3N_2O_4$ is unstable, which quickly decomposes into $C_2H_3NO_2$ and NO_2, and the former immediately decomposes into CH_2O and CHNO. This CH_2O soon decomposes to H and CHO. Although $C_2H_3N_2O_4$ forms earlier than other products, this is the only $C_2H_3N_2O_4$ formed during the whole heating process for PETNC. We did not observe the dissociation of $C_2H_3N_2O_4$ in the decomposition of Si-PETNC. The CH_2–O bond breaks just after $C_2H_3N_2O_4$ dissociation, leading to the formation of CHN_2O_4 at 2123 K (t = 13.5 ps). This CHN_2O_4 is also unstable, quickly decomposing to CO_2 and HN_2O_2. In comparison with Si-PETNC, CHN_2O_4 forms ~2 ps earlier and at a temperature of ~270 K lower for PETNC, making it more important in the initial decomposition of PETNC. The following reaction is H elimination from –NH at 2226 K (t = 14.27 ps), which is rapidly consumed by the attraction of the O in –CO within the same branch.

View Article Online
DOI: 10.1039/C7TA10998A

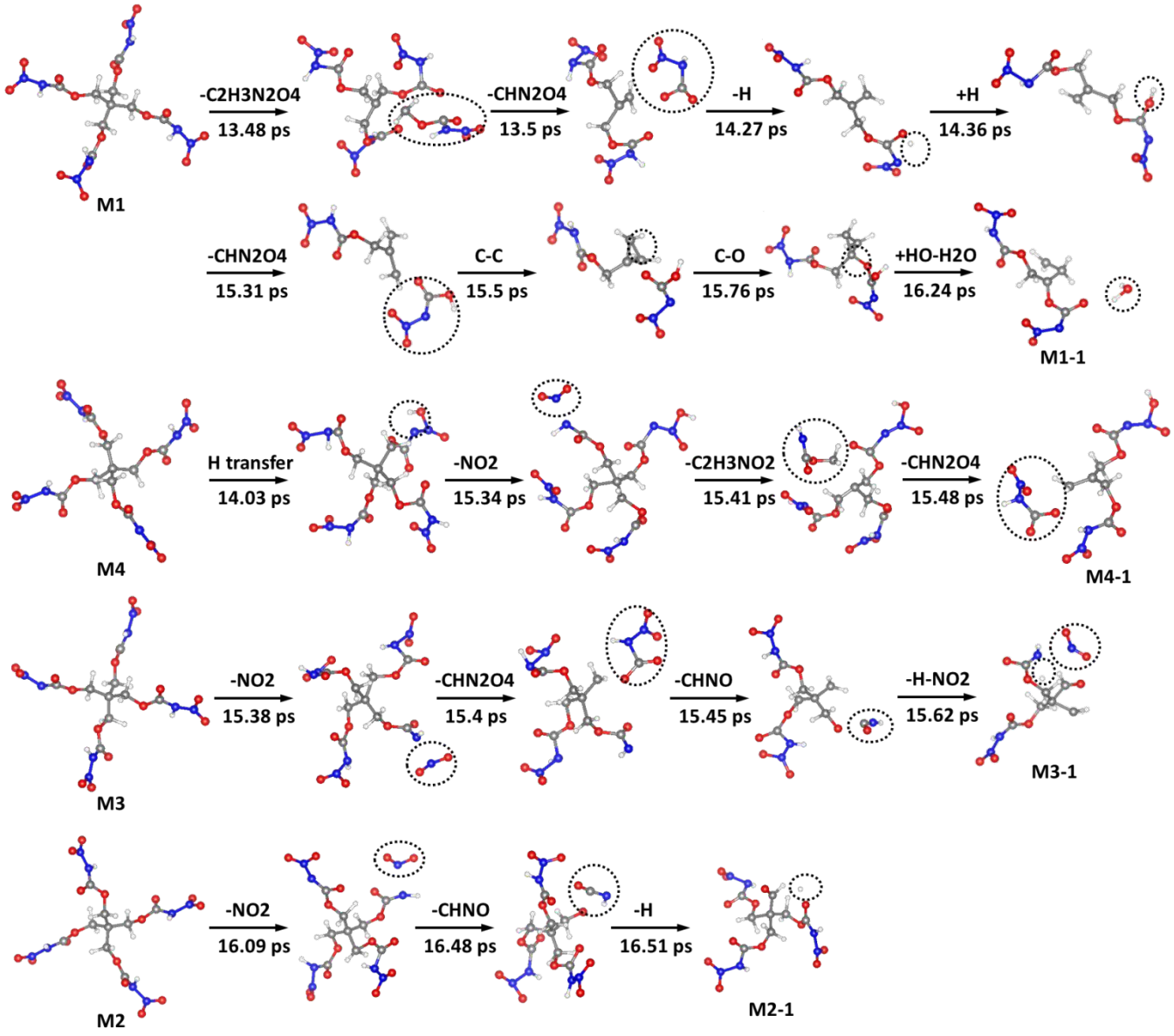

Fig. 6 Reaction process of initial reactions during the thermal decomposition of PETNC. The C, H, N, and O atoms are represented by gray, white, blue, and red balls, respectively.

For M4, the first reaction step is H transfer between the H in –NH and one O in $–NO_2$ when temperature approaches 2194 K (t = 14.03 ps). However, this H transfer does not promote the dissociation of HONO or HO. Instead, the decomposition of this molecule occurs through $NH–NO_2$ bond cleavage in another branch at 2371 K (t = 15.34 ps). This is identical to the intramolecular H transfer in Si-PETNC. The following reactions of $C–CH_2$ and $CH_2–O$ bond breakage occur quickly after NO_2 dissociation, leading to the formation of $C_2H_3NO_2$ and CHN_2O_4 at 15.41 and 15.48 ps, respectively. $C_2H_3NO_2$ is unstable, which immediately decomposes into CH_2O and CHNO. We did not observe

View Article Online
DOI: 10.1039/C7TA10998A

$C_2H_3NO_2$ in the thermal decomposition of Si-PETNC. The initiation of M3 and M2 decomposition occurs via NH–NO_2 bond rupture that generates NO_2 when temperature reaches 2376 K (t = 15.38 ps) and 2472 K (t = 16.09 ps), respectively. The subsequent reactions for M3 include the dissociations of CHN_2O_4, CHNO, H, and the second NO_2. For M2, CHNO and H eliminations are the next reactions. The reaction details about these initial products and their evolutions with temperature/time are described in Fig. S6 of the ESI.

Unlike Si-PETNC, only one C–O bond is formed during the whole thermal decomposition process of PETNC. It is formed due to the attraction between the central C and one O in the dissociated CHN_2O_4 when temperature reaches 2428 K (t = 15.76 ps) in one thoroughly decomposed PETNC molecule (M1 as shown in Fig. 6). No C–CH_2–O rearrangement is detected for PETNC due to the large branch that is difficult to bend and the high barrier of this reaction. Therefore, C–O bond formation does **not** play an important role in the decomposition of PETNC, which is a significant difference in the initial reactions between Si-PETNC and PETNC.

When temperature increases to ~2500 K, the increments of various intermediate products are detected, including HONO, $H_2N_2O_2$, $CH_2N_2O_4$, NO, HO, CNO, HNO, and N_2O_2. The further decompositions of initial products as well as PETNC moieties and the secondary reactions between products lead to the formations of these intermediates. The final products formed during the thermal decomposition of PETNC include CO_2, CO, H_2O, N_2O, H_2, and N_2. The evolutions of major reaction products with temperature/time are presented in Fig. S6 of the ESI.

3.3 The Origins for the Higher Sensitivity of Silicon Analogs and the Lower Sensitivity of Nitrocarbamates

Energetic molecular solids can rapidly transition from slow thermal decomposition to rapid, self-sustained reactions that lead to thermal runaway and explosion.[61,62] Because the initial decomposition is endothermic, the internal energy release and increased violence of reaction are delayed until the onset of exothermic reactions, which are thus of paramount importance to the safety of EMs.[63] We consider that the variation of energy under external stimuli is crucial to understand the sensitivity of EMs since it correlates closely with the violence of initial endothermic reactions and secondary exothermic reactions. Thus we consider that the temperature programmed reaction dynamics provides a more reliable measurement of sensitivity than considering just one or two specific factors such as molecular electronegativity and the weakest bond dissociation energy.

View Article Online
DOI: 10.1039/C7TA10998A

Fig. 7 shows the potential energy variations with temperature/time during the thermal decomposition process under heating for Si-PETN, PETN, Si-PETNC, and PETNC. For the nitro esters Si-PETN and PETN, the evolution of potential energy can be partitioned into two stages: the energy accumulation and then energy release. For Si-PETN, the energy increases from the beginning to ~11.3 ps and the corresponding temperature is 1826 K. The starting point of energy release agrees well with the time at which the rapid formation of Si–O bond begins. Considering that the other two reactions occurring before 11.3 ps (NO_2 and CH_2O dissociations) are endothermic, we conclude that the energy release is from Si–O bond formation. For PETN, the energy release starts from 13.9 ps and the corresponding temperature reaches 2177 K, which matches very well with the time after which many intermediate and final products are generated due to secondary exothermic reactions between products. Thus, the onset of energy release begins earlier and at a much lower temperature for Si-PETN, in comparison with PETN.

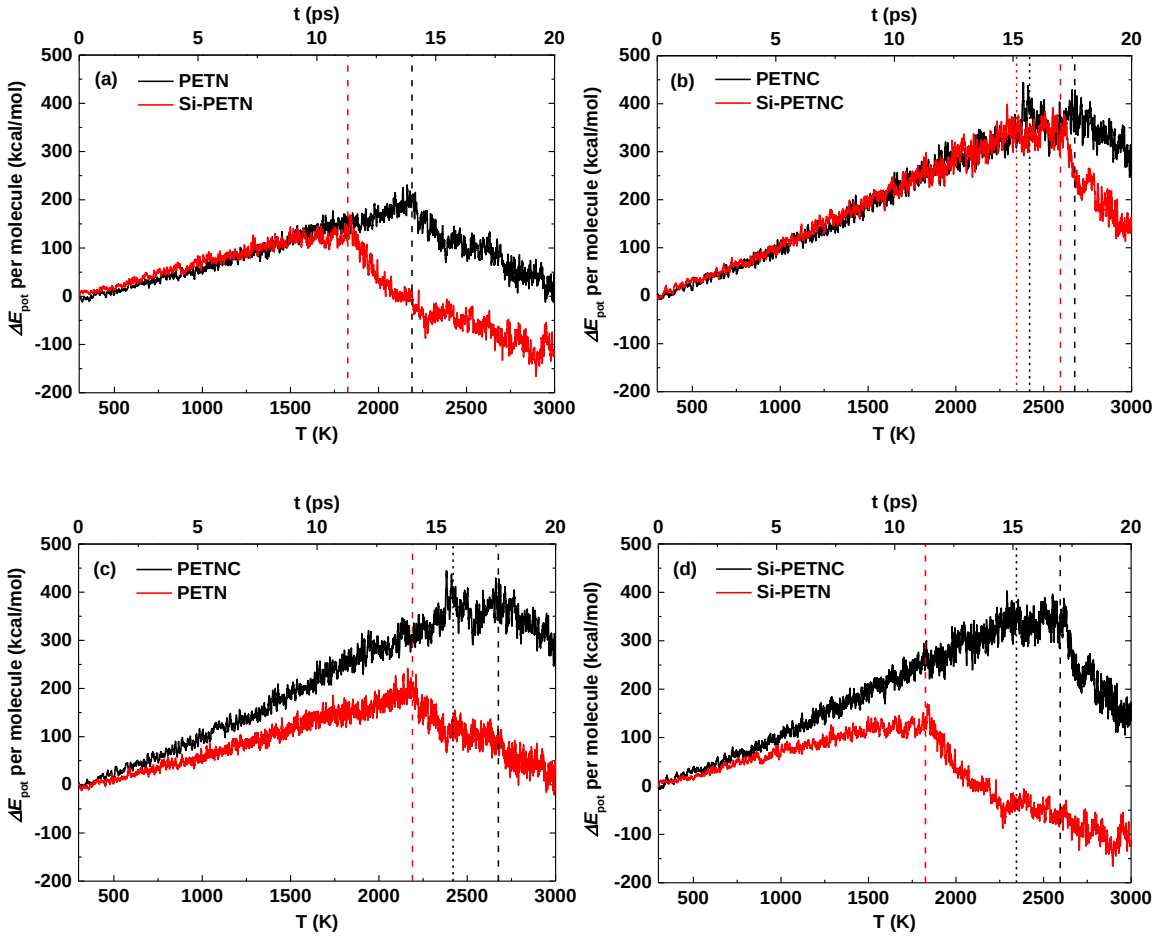

Fig. 7 Variation of potential energy with temperature/time during the thermal decompositions of Si-PETN, PETN, Si-PETNC, and PETNC. The data were normalized by the number of initial reactant molecules

View Article Online
DOI: 10.1039/C7TA10998A

Unlike the nitro esters, the evolutions of potential energy for the nitrocarbamates Si-PETNC and PETNC experience three stages: a long time increase in stage one followed by a short dynamical equilibrium in stage two and a decrease in stage three. For Si-PETNC, the energy increases within the first 15.15 ps (T = 2345 K) due to various initial endothermic reactions, followed by a dynamical equilibrium over the next 1.85 ps since some exothermic reactions occur. The energy begins to decrease after 17.0 ps (T = 2595 K), in excellent agreement with the time after which the rapid formation of Si–O bonds starts, indicating that Si–O bond formation contributes significantly to the energy release of Si-PETNC. For PETNC, the first stage lasts for 15.7 ps (T = 2420 K), followed by a dynamical equilibrium during the next 1.9 ps. The energy begins to release after 17.6 ps (T = 2676 K) due to the onsets of more exothermic reactions that generate more intermediate and final products. Therefore, the energy releases earlier and at a lower temperature for Si-PETNC than that for PETNC, which is consistent with the comparison between Si-PETN and PETN.

The different behavior between the carbon and silicon analogs indicates that the replacement of the central C atom by Si atom accelerates thermal decomposition and energy release, making the Si analogs more sensitive. The high exothermicity of Si–O bond formation as an essential initial reaction in the decompositions of the Si analogs promotes the onset of other reactions including the decomposition of other products and the secondary reactions between products, leading to the generations of various intermediate and final products that release energy. This significantly accelerates the decomposition process and thus enhances the sensitivity.

Comparing the energy behaviors of the nitro esters and the nitrocarbamates, we find that the energy release begins much later and at much higher temperature for the nitrocarbamates. The starting time and temperature are 13.9 ps and 2177 K for PETN, while they are 17.6 ps and 2676 K for PETNC. The decomposition of Si-PETN begins to release energy after 11.3 ps and the temperature is 1826 K, whereas, the onset of energy release for Si-PETNC starts after 17.0 ps and the temperature approaches 2595 K. This indicates that the decomposition proceeds much more slowly and the exothermic reactions occur much later for the nitrocarbamates, making them less sensitive.

Table 3 The important initial reaction products formed during the thermal decompositions of Si-PETN, PETN, Si-PETNC, and PETNC. The corresponding formation time and temperature are included.

material	product	t (ps)	T (K)
Si-PETN	NO2	9.21	1543
	CH2O	9.25	1549

View Article Online
DOI: 10.1039/C7TA10998A

	Si-O bond	9.35	1562
PETN	NO2	13.17	2078
	HONO, H	13.24	2087
	CH2O	13.31	2097
Si-PETNC	H transfer	10.19	1676
	NO2	12.72	2017
	H, HONO, CNO, CHNO	14.80	2298
	Si-O bond	15.21	2353
PETNC	C2H3N2O4	13.48	2120
	CHN2O4	13.50	2123
	H transfer	14.03	2194
	H	14.27	2226
	NO2, CHNO, C2H3NO2	15.34	2371

Another significant distinction is that the energy accumulated in stage one of the nitrocarbamates is much higher than that for the nitro esters, suggesting that nitrocarbamates need more energy to break the bonds in initial reactions. This implies that the nitrocarbamates lead to more initial reaction pathways that absorb energy or that the reaction barriers for the initial reactions are higher. Indeed, more endothermic reaction routes are observed in the initial decompositions of PETNC and Si-PETNC, compared to PETN and Si-PETN as shown in Table 3. This arises from the large and complex branch of the nitrocarbamate compounds that triggers various reaction channels. The common reaction product NO_2 is observed in the initial decomposition for all four EMs, but the reaction barriers for the nitrocarbamates are much higher. The reaction enthalpy for O–NO_2 bond dissociation in PETN and Si-PETN are 39.0 and 35.6 kcal/mol,[24] while the reaction enthalpy for NH–NO_2 bond dissociation in PETNC and Si-PETNC approach to 48.6 and 48.2 kcal/mol with zero point energy (ZPE) correction from QM calculations at the level of M06/6-311G**. Hence, NO_2 is formed at a much higher temperature and the population is smaller for the nitrocarbamates than for the nitro esters, as compared in Fig. 8 (a). Furthermore, the intervals between two initial reactions for PETNC and Si-PETNC are longer than those for PETN and Si-PETN, indicating that early reactions for the nitrocarbamates may not catalyze following reactions and thus decomposition progresses more slowly. Although Si–O bond formation is observed for both Si-PETN and Si-PETNC, it occurs at a much higher temperature for Si-PETNC and the number is smaller as shown in Fig. 8 (b). This is due to the large branch in the nitrocarbamates, which makes it more difficult to bend and rearrange the Si–CH_2–O and also impedes the attraction between the central Si and the O in dissociated products. Therefore, the role of Si–O bond formation in enhancing sensitivity for Si-PETNC is much less remarkable than for Si-PETN, making it much less sensitive. The subsequent equilibrium stage for the nitrocarbamates shows that the energy absorbed by endothermic reactions is still competitive with that released by exothermic reactions. This

View Article Online
DOI: 10.1039/C7TA10998A

indicates that there are fewer secondary exothermic reactions or that the released energy is smaller for the nitrocarbamates, in comparison with the nitro esters.

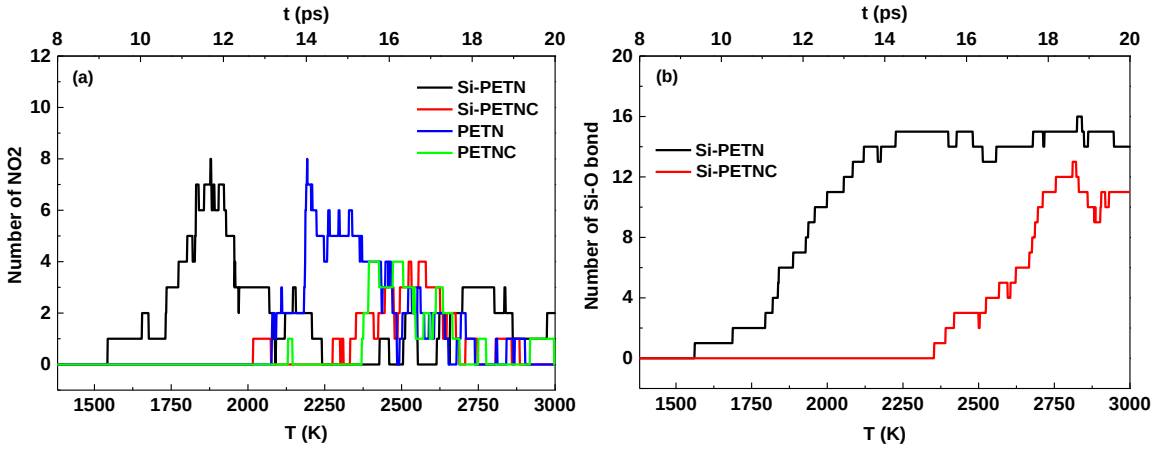

Fig. 8 Evolution with temperature/time of NO_2 and Si–O bond formed during the thermal decomposition of Si-PETN, PETN, Si-PETNC, and PETNC

3.4 Sensitivity Evaluation

Experimental measurements[23,27,28] collected in Table 4 for the four EMs suggest that

- thermal stability (T_{dec}) decreases as PETNC > Si-PETNC ≥ PETN > Si-PETN,
- impact sensitivity (IS) increases as PETNC < PETN ≤ Si-PETNC < Si-PETN, and
- friction sensitivity (FS) increases as PETNC < Si-PETNC < PETN < Si-PETN.

That is to say, subjected to the stimulus of thermal, impact, or friction, Si-PETN is always the most sensitive one, and PETNC is always the most stable one. The thermal stability and impact sensitivity for Si-PETNC are similar to those for PETN, but the former exhibits lower sensitivity to friction. Overall, these experimental data indicate that

- the relative sensitivity of the four EMs is: PETNC < Si-PETNC < PETN < Si-PETN.

Table 4 The relative sensitivity of PETN, PETNC, Si-PETN, and Si-PETNC

	Si-PETN	PETN	Si-PETNC	PETNC
t_{ini} (ps)	9.21	13.17	10.19	13.48
T_{ini} (K)	1543	2078	1676	2120
$t_{endo\text{-}exo}$ (ps)	11.30	13.90	17.0	17.60
$T_{endo\text{-}exo}$ (K)	1826	2177	2595	2676
ΔE_{endo} (kcal/mol)	156	210	389	430
r_{exo} (ps^{-1})	0.31	0.09	1.01	0.19

View Article Online
DOI: 10.1039/C7TA10998A

T_{dec} (K)	298[a]	438[b]	443[c]	469[b]
IS (J)		3~4[b]	3[c]	8[b]
FS (N)		60-80[b]	240[c]	360[b]

t_{ini}, T_{ini}: the initiation time and corresponding temperature of the first reaction step; $t_{endo\text{-}exo}$, $T_{endo\text{-}exo}$: the time/ temperature at which the energy changes from endothermic to exothermic; ΔE_{endo}: the absorbed energy before energy release; r_{exo}: the rate of energy release; *a* from Ref. 29, a significant degree of decomposition was observed after 12 hours in a solution of Si-PETN in 1,2-dichloroethane at 298 K; *b* from Ref. 27; *c* from Ref. 28; IS: impact sensitivity; FS: friction sensitivity; No experimental data about the IS and FS for Si-PETN are obtained due to its extraordinary high sensitivity.

Together with the experimental data regarding sensitivity, we summarized some crucial parameters obtained from the thermal decomposition simulations of Si-PETN, PETN, Si-PETNC, and PETNC in Table 4, trying to find the correlation between the parameters and the relative sensitivity of EMs. These parameters include the initiation temperature/time of the first reaction step (T_{ini} or t_{ini},), the temperature/time at which the energy changes from endothermic to exothermic ($T_{endo\text{-}exo}$ or $t_{endo\text{-}exo}$), the absorbed energy before energy release (ΔE_{endo}), and the rate of energy release (r_{exo}). We find that $T_{endo\text{-}exo}$ (or $t_{endo\text{-}exo}$) and ΔE_{endo} correlate very well with the relative sensitivity of the four EMs, as shown in Fig. 9. The EM with lower $T_{endo\text{-}exo}$ (or earlier $t_{endo\text{-}exo}$) and less ΔE_{endo} exhibits higher sensitivity, while the one with higher $T_{endo\text{-}exo}$ (or later $t_{endo\text{-}exo}$) and more ΔE_{endo} has lower sensitivity. Accordingly, our DFT-MD simulations suggest that

- the relative sensitivity of the four EMs is: PETNC < Si-PETNC < PETN < Si-PETN,

consistent with experimental result. Thus we recommend that the temperature/time at which the energy changes from endothermic to exothermic and the absorbed energy before energy release correlate with the relative sensitivity of EMs, providing a simple tool for predicting the sensitivity of novel EMs in advance of experimental synthesis and characterization. This criterion should provide guidance for developing new EMs with improved properties.

View Article Online
DOI: 10.1039/C7TA10998A

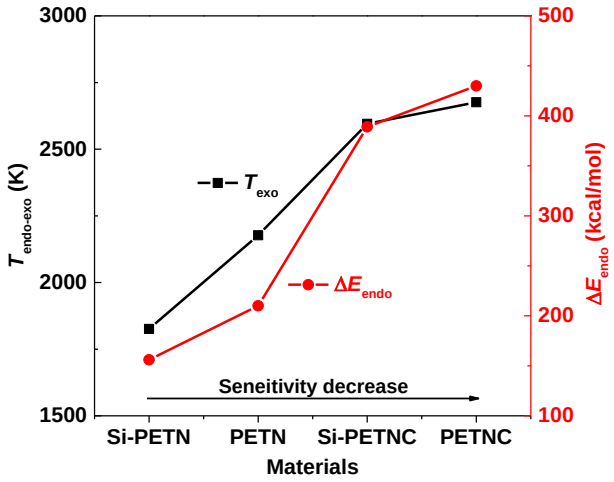

Fig. 9 Sensitivity correlation of the temperature at which the energy changes from endothermic to exothermic ($T_{endo-exo}$) and the absorbed energy before energy release (ΔE_{endo}) for Si-PETN, PETN, Si-PETNC, and PETNC. We find that $T_{endo-exo}$ and ΔE_{endo} both correlate very well with the relative sensitivity of the four EMs. The EM with lower $T_{endo-exo}$ and less ΔE_{endo} has higher sensitivity, while the one with higher $T_{endo-exo}$ and more ΔE_{endo} exhibits lower sensitivity.

The initiation temperature/time of the first reaction step does **not** correlate with relative sensitivity of the four EMs. For example, although the first reaction step occurs at a temperature of 400 K lower (or ~3 ps earlier) for Si-PETNC than that for PETN, the former is less sensitive. The first reaction step (H transfer) occurring in Si-PETNC does not catalyze other reactions, showing little effect on enhancing sensitivity. Therefore, we stress that it is necessary to find out whether the initial reaction promotes other reactions or not when using it to evaluate the sensitivity of EMs. The rate of energy release r_{exo} neither correlates with the sensitivity of these EMs. r_{exo} is higher for the nitrocarbamates than that for the nitro esters, which is opposite to the relative sensitivity.

4. Conclusions

We used DFT-MD based tempereature programmed reaction dynamics to determine the decomposition mechanisms of Si-PETN, PETN, Si-PETNC, and PETNC crystals to unravel the origins for the high sensitivity of Si analogs (Si-PETN, Si-PETNC) and the low sensitivity of nitrocarbamates (Si-PETNC, PETNC). We also find a simple analysis that predicts the relative sensitivity of EMs.

The critical initial reaction products for Si-PETN include NO_2, CH_2O, and Si–O bond. The mechanisms leading to the formation of Si–O bond involve the attraction between Si and the O from dissociated products, the rearrangement of Si–CH_2–O in the partially decomposed Si-PETN molecule, and the intermolecular and intramolecular attractions between Si and one O in –NO_2. The attraction

View Article Online
DOI: 10.1039/C7TA10998A

between Si and the O from dissociated products plays the predominant role in Si–O bond formation. The initial decomposition of PETN leads to the formations of NO_2, HONO, H, and CH_2O.

For Si-PETNC, the crucial initial reactions include hydrogen transfer, dissociations of NO_2, H, HONO, CNO, and CHNO, and Si–O bond formation. The intermolecular and intramolecular H transfers do not catalyze other reactions, and therefore do **not** accelerate the decomposition process. The mechanisms leading to the Si–O bond formation in Si-PETNC are similar to those in Si-PETN: the rearrangement of Si–CH_2–O in the partially decomposed Si-PETNC molecule, the attraction between Si and the O from dissociated fragments, and Si attracting the O pertaining to –CH_2O in the adjacent Si-PETNC residue. The attraction between Si and the O from dissociated fragments dominants the formation of Si–O bond in Si-PETNC, identical to that for Si-PETN. The initial reactions for PETNC include dissociations of $C_2H_3N_2O_4$ and CHN_2O_4, intramolecular hydrogen transfer, and eliminations of H, NO_2, $C_2H_3NO_2$, and CHNO. The H transfer does **not** promote other reactions, the same as that for Si-PETNC.

In comparison with PETN and PETNC, the higher sensitivity of the Si analogs originates from the highly exothermic Si–O bond formation as a paramount initial reaction. It promotes other reactions including the decompositions of initial products and the secondary exothermic reactions between products, leading to the generations of various intermediates and final products, thus accelerating the decomposition process and energy release and enhancing the sensitivity of Si-PETN and Si-PETNC.

The much lower sensitivity of nitrocabamates compared to nitro esters is due to the large and complex branch of the reactant molecules. This large branch makes it more difficult to bend and rearrange the Si/C–CH_2–O and also impedes the attraction between the central Si/C and the O in dissociated products. The Si–O bond forms at a higher temperature and the quantity is less for Si-PETNC compared to Si-PETN. The large complex branch also triggers more initial reaction channels that absorb energy and have higher reaction barrier. These factors delay the onsets of secondary reactions and energy release, thus lowering the sensitivity of Si-PETNC and PETNC.

The changes in potential energy under external stimuli provides an important measure for evaluating the sensitivity of EMs since it correlates closely with initial endothermic reactions and secondary exothermic reactions. We find that the temperature/time at which the energy changes from endothermic to exothermic ($T_{\text{endo-exo}}$ or $t_{\text{endo-exo}}$) and the accumulated energy before energy release (ΔE_{endo}) correlate very well with the relative sensitivity of the four EMs, making them useful criteria. The EM with lower

View Article Online
DOI: 10.1039/C7TA10998A

$T_{endo\text{-}exo}$ (or earlier $t_{endo\text{-}exo}$) and less ΔE_{endo} has higher sensitivity, while the one with higher $T_{endo\text{-}exo}$ (or later $t_{endo\text{-}exo}$) and more ΔE_{endo} exhibits lower sensitivity. Accordingly, the relative sensitivity of the four EMs predicted by our dynamical simulations is PETNC < Si-PETNC < PETN < Si-PETN, consistent with experimental results.

This study explains the increased sensitivity of Si analogs and the decreased sensitivity of nitrocarbamates of energetic molecules, providing mechanistic insight on the molecular and structural determinants that control sensitivity of EMs. The proposed criteria related to energy variation under external stimulus provide a practical approach to predict the relative sensitivity of EMs in advance of experimental synthesis and characterization. These findings should be useful in developing novel EMs with improved properties.

Conflicts of interest

The authors declare no conflicts of interest.

Acknowledgements

This work was supported by the National Natural Science Foundation of China (Grant No. 11402031 and 11521062) and by ONR (N00014-12-1-0538, Cliff Bedford program manager).

Notes

† Electronic Supplementary Information (ESI) available: The equilibrium cell parameters for PETN, Si-PETN, PETNC, and Si-PETNC crystals predicted from PBE-D3 calculations at zero temperature are collected in Table S1. Bond order cutoff values for various atom pairs used to identify molecular fragments in PETN, Si-PETN, PETNC, and Si-PETNC are tabulated in Table S2~S5. Evolution with temperature/time of the reaction products formed during the thermal decomposition of Si-PETN is plotted in Fig. S1. Molecular structures before and after Si–O bond formation during the thermal decomposition of Si-PETN are illustrated in Fig. S2. Evolution with temperature/time of the reaction products formed during the thermal decomposition of PETN is shown in Fig. S3. Evolution with temperature/time of the reaction products formed during the thermal decomposition of Si-PETNC is presented in Fig. S4. Molecular structures before and after Si–O bond formation during the thermal decomposition of Si-PETNC are shown in Fig. S5. Evolution with temperature/time of the reaction products formed during the thermal decomposition of PETNC is plotted in Fig. S6.

References

1 T. M. Klapötke, *Chemistry of High-Energy Materials*, 3rd ed., De Gruyter, Berlin, 2015.

View Article Online
DOI: 10.1039/C7TA10998A

2 T. Brinck, *Green Energetic Materials*, Wiley, New York, 2014.

3 J. P. Agrawal, *High Energy Materials: Propellants, Explosives and Pyrotechnics*, Wiley-VCH, Weinheim, 2010.

4 J. Giles, *Nature*, 2004, **427**, 580–581.

5 (a) A. A. Dippold and T. M. Klapötke, *J. Am. Chem. Soc.* 2013, **135**, 9931–9938. (b) M. Göbel, B. H. Tchitchanov, J. S. Murray, P. Politzer and T. M. Klapötke, *Nature Chem*., 2009, **1**, 229–235. (c) T. M. Klapötke, C. Ptermayer, D. G. Pierey and J. Stierstofer, *J. Am. Chem. Soc.* 2012, **134**, 20827–20836. (d) D. Fischer, J. L. Gottfried, T. M. Klapötke, K. Karaghiosoff, J. Stierstorfer and T. G. Witkowski, *Angew. Chem. Int. Ed.* 2016, **55**, 16132–16135. (e) T. S. Hermann, K. Karaghiosoff, T. M. Klapötke and J. Stierstorfer, *Chem. Eur. J.*, 2017, **23**,12087–12091.

6 (a) H. Gao and J. M. Shreeve, *Chem. Rev*. 2011, **111**, 7377–7436. (b) J. Zhang, Q. Zhang, T. T. Vo, D. A. Parrish and J. M. Shreeve, *J. Am. Chem. Soc.* 2015, **137**, 1697−1704. (c) Y. Liu, J. Zhang, K. Wang, J. Li, Q. Zhang and J. M. Shreeve, *Angew. Chem. Int. Ed.* 2016, **55**, 11548–11551. (d) P. Yin, J. Zhang, L. A. Mitchell, D. A. Parrish, J. M. Shreeve, *Angew. Chem. Int. Ed.* 2016, **55**, 12895–12897. (e) Y. Tang, J. Zhang, L. A. Mitchell, D. A. Parrish and J. M. Shreeve, *J. Am. Chem. Soc.* 2015, **137**, 15984−15987. (f) V. Thottempudi, H. Gao and J. M. Shreeve, *J. Am. Chem. Soc*., 2011, **133**, 6464–6470.

7 W. Zhang, J. Zhang, M. Deng, X. Qi, F. Nie and Q. Zhang, *Nat Commun*., 2017, **8**, 1–7.

8 D. G. Piercey, D. E. Chavez, B. L. Scott, G. H. Imler and D. A. Parrish, *Angew. Chem. Int. Ed.* 2016, **55**, 15315–15318.

9 C. Zhang, C. Sun, B. Hu, C. Yu and M. Lu, *Science*, 2016, **355**, 374–376.

10 G. Bélanger-Chabot, M. Rahm, R. Haiges and K. O. Christe, *Angew. Chem. Int. Ed*. 2015, **127**, 11896–11900.

11 Y. Tang, H. Yang, B. Wu, X. Ju, C. Lu and G. Cheng, *Angew. Chem., Int. Ed.* 2013, **52**, 4875–4877.

12 U. Teipel, *Energetic Materials. Particle Processing and Characterization*, WILEY-VCH Verlag GmbH & Co. KGaA, 2005.

13 S. Iyer and N. Slagg, In *Structure and reactivity*, ed. J. F. Liebman and A. Greenberg, VCH, New York, 1988, ch 7.

14 C. B. Storm, J. R. Stine and J. F. Kramer, In *Chemistry and physics of energetic materials*, ed. S. N. Bulusu, Kluwer, Dordrecht, The Netherlands, 1990, ch 27.

15 R. Meyer, J. Köhler and A. Hornburg, *Explosives*, 6th ed., Wiley-VCH, Weinheim, 2007.

16 T. Zhou, J. Lou, Y. Zhang, H. Song and Fenglei Huang, *Phys. Chem. Chem. Phys*., 2016, **18**, 17627–17645.

17 C. Deng, X. Xue, Y. Chi, H. Li, X. Long and C. Zhang, *J. Phys. Chem. C*, 2017, **121**, 12101–12109.

18 Y. Ma, A. Zhang, X. Xue, D. Jiang, Y. Zhu and C. Zhang, *Cryst. Growth Des.* 2014, **14**, 6101–6114.

19 J. Zhang, L. A. Mitchell, D. A. Parrish and J. M. Shreeve, *J. Am. Chem. Soc*., 2015, **137**, 10532–10535.

20 V. J. Bellitto and M. I. Melnik, *Appl. Surf. Sci.*, 2010, **256**, 3478–3481.

21 H. Czerski and W. G. Proud, *J. Appl. Phys*., 2007, **102**, 113515.

22 M. Huang, H. Z. Li, R. Xu, X. Q. Zhou, F. D. Nie and B. Chen, *Chin. J. Energ. Mater*., 2011, **19**, 621–626.

23 T. M. Klapötke, B. Krumm, R. Ilg, D. Troegel and R. Tacke. *J. Am. Chem. Soc*., 2007, **129**, 6908–6915.

24 W.-G. Liu, S.V. Zybin, S. Dasgupta, T. M. Klapötke and W. A. Goddard III, *J. Am. Chem. Soc*., 2009, **131**, 7490–7491.

25 T. Zhou, L. Liu, W.A. Goddard III, S. V. Zybin and F. Huang, *Phys. Chem. Chem. Phys*., 2014, **16**, 23779–23791.

26 B. W. Asay, B. F. Henson, L. B. Smilowitz and P. M. Dickson, *J. Energ. Mater*., 2003, **21**, 223–235.

27 Q. J. Axthammer, B. Krumm and T. M. Klapötke, *Eur. J. Org. Chem.*, 2015, 723–729.

28 Q.J. Axthammer, T. M. Klapötke, B. Krumm and T. Reith, *Inorg. Chem*. 2016, **55**, 4683−4692.

29 D. D. Dlott, *Mater. Sci. Technol*. 2006, **22**, 463–473.

View Article Online
DOI: 10.1039/C7TA10998A

30 R. W. Armstrong, B. Baschung, D. W. Booth and M. Samirant, *Nano Lett.* 2003, **3**, 253–255.

31 (a) J. T. Mang, R. P. Hjelm and E. G. Francois, *Propellants, Explos., Pyrotech*., 2010, **35**, 7–14. (b) J. T. Mang and R. P. Hjelm, *Propellants, Explos., Pyrotech.,* 2011, **36**, 439–445.

32 Q. An, W. A. Goddard III, S. V. Zybin, A. J. Botero and T. T. Zhou, *J. Phys. Chem. C*, 2013, **117**, 26551–26561.

33 O. Sharia and M. Kuklja, *J. Am. Chem. Soc*., 2012, **134**, 11815−8365.

34 M. J. Kamlet and H. G. Adolph, *Propellants, Explosives, Pyrotechnics*, 1979, **4**, 30–34.

35 (a) S. Zeman, In *Structure and Bonding*, ed. D. M. P. Mingos, Springer, Berlin, 2007. (b) S. Zeman, *J Hazard Mater A*, 2006, **132**, 155–164.

36 (a) P. Politzer and J. S. Murray, *Energetic Materials: Theoretical and Computational Chemistry Series*, Vol. 12, Elsevier, New York, 2003. (b) P. Politzer and J. S. Murray, In *Energetic Materials, Part 2. Detonation, Combustion*, ed. P. Politzer and J. S. Murray, Elsevier, Amsterdam, 2003. (c) P. Politzer, J. S. Murray, *J Mol Struct*, 1996, 376, 419–424. (d) J. S. Murray, M. C. Concha and P. Politzer, *Mol Phys.*, 2009, 107, 89–97. (e) P. Politzer, J. S. Murray, J. M. Seminario, P. Lane, M. E. Grice and M. C. Concha, *J Mol Struct (Theochem)*, 2001, 573, 1–10. (f) J. O. Oxley, In: *Energetic materials, part 1. Decomposition, crystal and molecular properties*, ed. P. Politzer and J. S. Murray, 2003, Elsevier, Amsterdam, ch 1.

37 (a) M. Pospíšil, P. Vávra, M. C. Concha, J. S. Murray and P. Politzer, *Journal of Molecular Modeling*, 2010, **16**, 895–901. (b) M. Pospíšil, P. Vávra, M. C. Concha, J. S. Murray and P. Politzer, *J Mol Model*, 2011, **17**, 2569–2574

38 (a) L. E. Fried, M. R. Manaa, P. F Pagoria and R. L. Simpson. *Annu. Rev. Mater. Res*., 2001, **31**, 291–321. (b) S. M. Walley, J. E. Field and M. W. Greenaway, *Materials Science and Technology*, 2006, **22**, 402–413. (d) C. J. Wu and L. E. Fried, *Proceed. 11th Int. Symp. Detonation*, Snowmass, CO, 1998.

39 (a) H. M. Xiao, W. H. Zhu, J. J. Xiao, G. X. Wang and X. Q. Pei, *Chinese Journal of Energetic Materials*, 2012, **20**, 514. (b) W. Zhu and H. Xiao, *Struct Chem*, 2010, **21**, 657–665. (c) W. H. Zhu and H. M. Xiao, *J Phys. Chem. B*, 2009, 113, 10315–10321.

40 (a) E. A. Zhurova, A. Martin and A. A. Pinkerton, *J. Am. Chem. Soc*., 2002, **124**, 8741–8750. (b) J. P. Ritchie, E. A. Zhurova, A. Martin and A. A. Pinkerton, *J. Phys. Chem*., 2003, **B107**, 14576–14589.

41 B. M. Rice and J. J. Hare, *J Phys. Chem. A*, 2002, **106**, 1770–1783.

42 D. Mathieu, *Ind. Eng. Chem. Res.*, 2017, **56**, 8191–8201.

43 S. A. Shackelford, *Central European Journal of Energetic Materials*, 2008, **5**, 75–101.

44 M. H. Keshavarz and M. Jaafari, *Propellants, Explosives, Pyrotechnics*, 2006, **31**, 216–225.

45 J. A. Morrill and E. F. C. Byrd, *Journal of Molecular Graphics and Modelling*, 2008, **27**, 349–355.

46 M. M. Kuklja, Quantum-Chemical Modeling of Energetic Materials: Chemical Reactions Triggered by Defects, Deformations, and Electronic Excitations. *Adv. Quantum Chem*., 2014, **68**, 71–146.

47 J. Trotter, Bond lengths and angles in pentaerythritol tetranitrate, *Acta Crystallographica*, 1963, **16**, 698–699.

48 (a) W. Kohn, L. J. Sham, Self-Consistent Equations Including Exchange and Correlation Effects, *Phys. Rev*., 1965, **140**, A1133. (b) P. Hohenberg and W. Kohn, Inhomogeneous Electron Gas, *Phys. Rev. B*, 1964, **136**, B864.

49 J. P. Perdew, K. Burke and M. Ernzerhof, *Phys. Rev. Lett*. 1996, **77**, 3865−3868.

50 S. Grimme, S. Ehrlich and L. Goerigk, *J. Comp. Chem.*, 2011, **32**, 1456–1465.

51 (a) G. Kresse and J. Non-Cryst, *Solids*, 1995, **193**, 222–229. (b) G. Kresse and J. Furthmuller, *Comput. Mater. Sci*., 1996, **6**, 15–50. (c) G. Kresse and J. Furthmuller, *Phys. Rev. B: Condens. Matter Mater. Phys.*, 1996, **54**, 11169–11186. (d) G.

View Article Online
DOI: 10.1039/C7TA10998A

Kresse and D. Joubert, *Phys. Rev. B: Condens. Matter Mater. Phys*., 1999, **59**, 1758–1775. (e) M. Hacene, A. Anciaux-Sedrakian, X. Rozanska, D. Klahr, T. Guignon and P. Fleurat-Lessard, *J. Comput. Chem*., 2012, **33**, 2581–2589. (f) M. Hutchinson and M. Widom, *Computer Physics Communications*, 2012, **183**, 1422–1426.

52 Q. An, Y. Liu, S. V. Zybin, H. Kim and W. A. Goddard III, *J. Phys. Chem. C*, 2012, **116**, 10198–10206.

53 Y. Lin, M. M. Budzevich, A. C. Landerville, I. I. Oleynik and C. T. White, *AIP Conference Proceedings*, 2009, **1195**, 474–477.

54 Y. A. Gruzdkov and Y. M. Gupta, *J. Phys. Chem. A*, 2000, **104**, 11169–11176.

55 W. L. Ng, J. E. Field and H. M. Hauser, *J. Appl. Phys*. 1986, **59**, 3945–3952.

56 D. L. Naud and K. R. Brower, *J. Org. Chem*. 1992, **57**, 3303–3308.

57 M. A. Hiskey, K. R. Brower and J. C. Oxley, *J. Phys. Chem*., 1991, **95**, 3955–3960.

58 R. Behrens, *J. Phys. Chem.*, 1990, **94**, 6706–6718.

59 J. C. Oxley, M. Hiskey, D. Naud and R. Szekeres, *J. Phys. Chem*., 1992, **96**, 2505–2509.

60 R. Behrens and S. Bulusu, *J. Phys. Chem*., 1992, **96**, 8877–8891.

61 G. F. Adams and R. W. Shaw, *Annu. Rev. Phys. Chem*., 1992, **43**, 311–340.

62 B. F. Henson and L. B. Smilowitz, In *Non-Shock Initiation of Explosives*, ed. B. W. Asay, Springer-Verlag, Berlin, 2010, p45–128.

63 V. I. Schweigert and S. E. Koh-Fallet, *J. Phys. Chem. A,* 2017, **121**, 1544−1552.

View Article Online
DOI: 10.1039/C7TA10998A

Table of content

Reaction Mechanisms and Sensitivity for Silicon Nitrocarbamate and Related Systems from Quantum Mechanics Reaction Dynamics

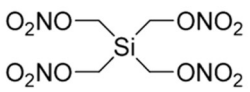

Si-PETN

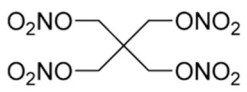

PETN

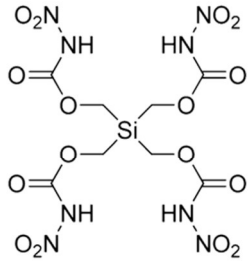

Si-PETNC

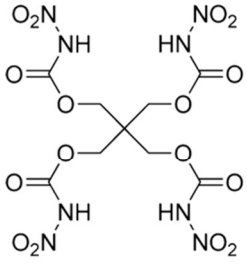

PETNC

The intramolecular differences of the four compounds lead to significant distinctions in the reaction mechanisms and sensitivity under heating